Thickness effect on solar-blind photoelectric properties of ultrathin β-Ga_2O_3 films prepared by atomic layer deposition

Shao-Qing Wang(王少青)[1], Ni-Ni Cheng(程妮妮)[1], Hai-An Wang(王海安)[1], Yi-Fan Jia(贾一凡)[1], Qin Lu(陆芹)[1], Jing Ning(宁静)[2], Yue Hao(郝跃)[2], Xiang-Tai Liu(刘祥泰)[1,†], and Hai-Feng Chen(陈海峰)[1,‡]

[1] *The Key Laboratory of Advanced Semiconductor Devices and Materials, Xi'an University of Posts & Telecommunications, Xi'an* 710121, *China*
[2] *The State Key Discipline Laboratory of Wide Band Gap Semiconductor Technology, Xidian University, Xi'an*, 710071, *China*

(Received 15 July 2022; revised manuscript received 24 August 2022; accepted manuscript online 26 August 2022)

The β-Ga_2O_3 films with different thicknesses are prepared by an atomic layer deposition system. The influence of film thickness on the crystal quality is obvious, indicating that the thicker films perform better crystal quality, which is verified from x-ray diffraction (XRD) and scanning electron microscope (SEM) results. The Ga_2O_3-based solar blind photodetectors with different thicknesses are fabricated and studied. The experimental results show that the responsivity of the photodetectors increases exponentially with the increase of the film thickness. The photodetectors with inter-fingered structure based on 900 growth cycles β-Ga_2O_3 active layers (corresponding film thickness of 58 nm) exhibit the best performances including a low dark current of 134 fA, photo-to-dark current ratio of 1.5×10^7, photoresponsivity of 1.56 A/W, detectivity of 2.77×10^{14} Jones, and external quantum efficiency of 764.49% at a bias voltage of 10 V under 254-nm DUV illumination. The photoresponse rejection ratio (R_{254}/R_{365}) is up to 1.86×10^5. In addition, we find that the photoelectric characteristics also depend on the finger spacing of the MSM structure. As the finger spacing decreases from 50 μm to 10 μm, the photoresponsivity, detectivity, and external quantum efficiency increase significantly.

Keywords: β-Ga_2O_3, film thickness, solar blind photodetectors, photoelectric response

PACS: 85.60.Gz, 81.15.Gh, 73.63.Bd **DOI:** 10.1088/1674-1056/ac8ce9

1. Introduction

Gallium oxide (Ga_2O_3) has ultra-wide band gap width (4.6 eV–4.9 eV), high critical electric field intensity (8 MV·cm^{-1}) and excellent chemical stability,[1] which makes it widely used in the fields of high-power electronic devices,[2,3] solar blind ultraviolet photodetectors,[4] and gas sensors.[5] Five crystalline forms of gallium oxide named α, β, γ, δ, and ε are found, among which β-Ga_2O_3 is the most stable in physical and chemical properties.[6] The β-Ga_2O_3 has high optical transmittance in the visible region (400 nm–800 nm) and excellent light absorption characteristics in the solar blind region (200 nm–280 nm), so they are widely used in the solar-blind photodetectors.[7,8] At present, there are many methods to prepare gallium oxide films, such as metal–organic chemical vapor deposition (MOCVD),[9] pulse laser deposition (PLD),[10] molecular beam epitaxy (MBE),[11] mist-chemical vapor deposition (Mist-CVD),[12] and magnetron sputtering (PVD).[13] So far, several groups have studied the influence of the film thickness on the photoelectric performance of β-Ga_2O_3 photodetectors. Li *et al.* prepared solar blind photodetectors based on β-Ga_2O_3 thin films with various thickness (150 nm–2.7 μm), which were grown on sapphire substrate by pulsed laser deposition technique.[12] It was found that with the film thickness increasing, the crystal quality gradually improved. When the film thickness was 250 nm, the β-Ga_2O_3 ultraviolet photoelectric detector (PD) had the highest photo-dark current ratio (PDCR) of 6.04×10^4.[14] Zhang *et al.*[15] fabricated UV detectors based on Ga_2O_3 films of different thicknesses (90 nm–354 nm) grown by PLD, and obtained ultra-high PDCR of 10^8 and ultra-low dark current of 100 fA when the film thickness was 298 nm. An *et al.*[16] prepared Ga_2O_3 films of different thicknesses by using radio frequency magnetron sputtering technology. They found that the β-Ga_2O_3 photodetector with a thickness of 200 nm exhibited higher photoresponse, faster rise time (1.0 s/1.4 s), and fall time (1.2 s/1.3 s). Li *et al.* fabricated β-Ga_2O_3 UV photodetectors with the thickness of 210 nm–1050 nm by PVD method. They found that the detection performance initially increases and then decreases with the film thickness increasing. When the β-Ga_2O_3 film thickness was 840 nm, the β-Ga_2O_3 ultraviolet showed the best photoelectric performance.[17]

Although some researchers have investigated the effects of Ga_2O_3 film thickness on the microstructure and photoelectrical properties, the effect of ultrathin Ga_2O_3 film (< 80 nm) on ultraviolet photodetector has not been studies yet. In this work, the β-Ga_2O_3 thin films with different thicknesses (18 nm–58 nm) grown by atomic layer deposition are characterized by ultraviolet-visible spectroscopy (UV-Vis), scanning electron microscope (SEM), and x-ray diffraction (XRD).

†Corresponding author. E-mail: liuxiangtai@xupt.edu.cn
‡Corresponding author. E-mail: chenhaifeng@xupt.edu.cn

© 2023 Chinese Physical Society and IOP Publishing Ltd

Then, all the films were fabricated into metal–semiconductor–metal (MSM) solar-blind photodetectors with inter-fingered structure to investigate the photoelectric characteristics. Finally, the thickness of active layer and size effect of MSM structure on photoelectrical properties of β-Ga_2O_3 solar blind PDs are discussed.

2. Experiment

In this work, Ga_2O_3 films were grown on sapphire substrates by atomic layer deposition process (8-inch (1 inch = 2.54 cm) waferscale, Veeco, PEALD system). The trimethylgallium (TMG) and ozone (O_3) were used as Ga-precursor and oxygen source, respectively. The TMG precursor was stored in a canister at room temperature. The working pressure was $\sim$ 0.14 Torr (1 Torr = 1.33322×10^2 Pa). As shown in Fig. 1(a), the typical ALD sequence consisted of four steps: Ga-precursor exposure (0.015 s), Ar gas purge (5 s), ozone exposure (5 s), and Ar gas purge (10 s) with the sample station temperature of 250 °C. The Ar purge flow was set to 20 sccm. After ALD growth, these films were annealed at 900 °C for 1 h in a high temperature tube furnace in air/N_2 mixture atmosphere. In order to study the influence of Ga_2O_3 thickness on photodetectors, the number of growth cycles was set to 300, 600, and 900, separately. The thickness of thin film measured by spectroscopic ellipsometry was 58 nm for 900 cycles, so the growth rate calculated is about 0.64 Å/cycle. The x-ray 7000 diffraction was used to analyze the crystallinity of the prepared Ga_2O_3 thin films. The surface morphology was observed by scanning electron microscopy (JSM-7610F Plus, JEOL). The transmittance and absorbance were obtained by UV-Vis spectroscopy (UV-2300, SHIMADZU).

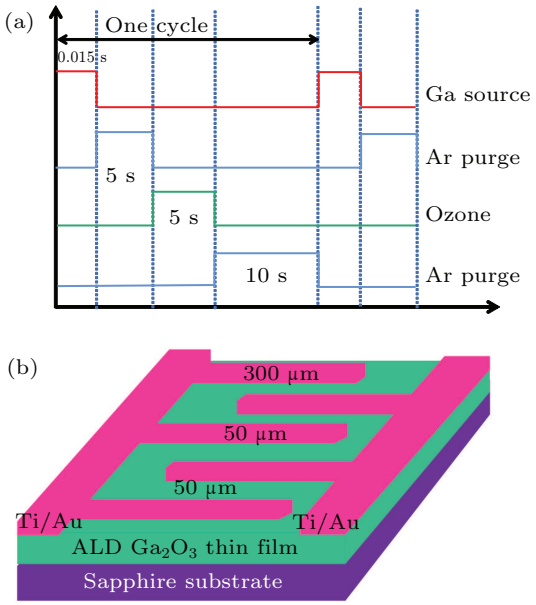


Fig. 1. (a) Schematic diagram of thin film deposition by ALD process, with one deposition cycle consisting of four steps: $Ga(CH_3)_3$ vapor pulse for 0.015 s, Ar purge gas for 5 s, ozone pulse for 5 s, and Ar purge gas for 10 s. (b) Schematic diagram of fabricated MSM structured UV solar blind photodetector.

After characterizing the structures and measuring the light transmittances of the prepared Ga_2O_3 films, the metal–semiconductor–metal (MSM) solar blind photodetectors were fabricated. Figure 1(b) shows that Ti/Au (80 nm/50 nm) electrodes are evaporated on the Ga_2O_3 thin films after being processed by a standard photolithography. Finally, MSM photodetectors were fabricated through a conventional lift-off process. The current–voltage (I–V) and time-dependent characteristics of the photodetectors were measured by a Keysight B1505A semiconductor analyzer. The photocurrents were measured under 254-nm DUV illumination with an intensity of 1000 μW/cm^2.

3. Results and discussion

3.1. Characterization of Ga_2O_3 films grown on sapphire substrates

To analyze the crystal structure of Ga_2O_3 film, the XRD spectra of the grown Ga_2O_3 films were obtained in grazing incidence XRD (GIXRD) mode, with a grazing angle δ of 0.5° as shown in Fig. 2. There is no signal peak from substrate in grazing incidence diffraction mode. The number of growth cycles for sample 1, sample 2, and sample 3 are 300, 600, and 900, respectively.

As shown in Fig. 2, all the peaks but for the one peak around 28.2° correspond to the x-ray diffraction pattern of β-Ga_2O_3 (PDF card No. 41-1103). The XRD diffraction peak around 28.2° is matched with the ε-Ga_2O_3 (PDF card No. 06-0509), which indicates that there is a small amount of ε-phase Ga_2O_3 nanocrystalline forming in sample 1. However, no ε-phase nanocrystalline forms in sample 3. Therefore, the films prepared by ALD process in our study mainly are of polycrystalline β-Ga_2O_3 after annealing in furnace tube at 900° for 60 min. For the three samples, the main diffraction peaks of β-Ga_2O_3 phase (-201) (18.9°) and (-202) (31.7°) turn stronger and sharper with the cycle number increasing. The decrease of the full width at half maximum (FWHM) of these peaks indicates that the grain size of β-Ga_2O_3 increases with the increase of film thickness.[18]

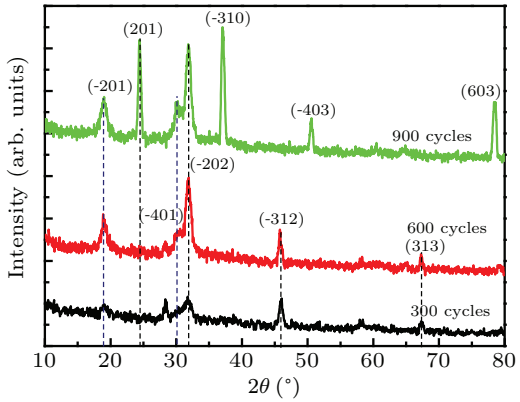


Fig. 2. XRD patterns of β-Ga_2O_3 films after being annealed at 900 °C for 60 min.

Figure 3 shows the FE-SEM images of three samples after being ex-situ annealed at 900° for 60 min. The size of crystal grains increase apparently with the increase of growth cycles. Combining the SEM images with the XRD analysis, we can conclude that the crystal quality of β-Ga_2O_3 film is improved with the increase of film thickness.

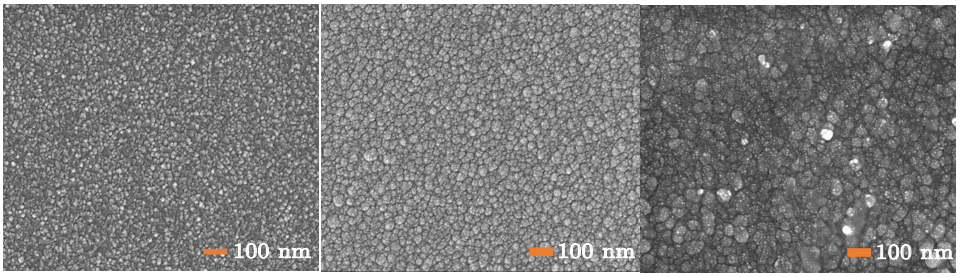


Fig. 3. FE-SEM images of (a) sample 1, (b) sample 2, and (c) sample 3.

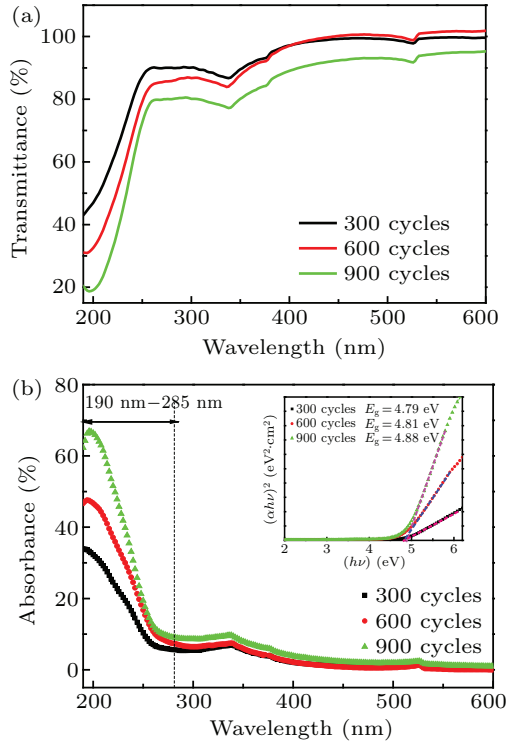


Fig. 4. (a) Optical transmission spectra and (b) absorption spectra of prepared β-Ga_2O_3 films with different growth cycles, with inset showing Tauc plots of prepared Ga_2O_3 thin film.

Figure 4(a) shows the curves of transmittance *versus* wavelength of the β-Ga_2O_3 thin films grown for different cycles, which is measured by using UV-Vis spectroscopy in a wavelength range from 190 nm to 800 nm. All the thin films show outstanding optical transmission (over 85% in visible light range). For the three samples, the transmittance decreases gradually with the cycle number increasing in the ultraviolet band from 200 nm to 400 nm. Figure 4(b) indicates that β-Ga_2O_3 films have obvious UV absorptions in a solar blind range of 200 nm–280 nm. The inset of Fig. 4(b) shows the curves of the relative absorption coefficient $(\alpha h\nu)^2$ against the photon energy $h\nu$. A sharp absorption edge is observed. As β-Ga_2O_3 is a material with a direct band gap, the value of optical bandgap E_g can be estimated by extrapolating the linear section of the plot to energy axis according to the formula[19]

$$\alpha h\nu \propto \left(h\nu - E_g\right)^{1/2}, \tag{1}$$

where α is the absorption coefficient and $h\nu$ is the photon energy. The optical bandgap is 4.79 eV for sample 1, 4.81 eV for sample 2, and 4.88 eV for sample 3, separately. The optical band gaps show a slight increase as the number of deposition cycles increases. As the film thickness increases, the strain caused by the lattice mismatch with sapphire substrate decreases, resulting in the slight increase of the band gap.[19]

3.2. Photoelectric characteristic analysis

In order to study the optoelectrical properties of β-Ga_2O_3 films for the three samples, metal–semiconductor–metal (MSM) photodetectors are fabricated on these films. The 5 pairs of Ti/Au (80 nm/50 nm) interdigitated electrodes with 300 μm in length, 50 μm in width, and 50 μm in space were fabricated by using the standard photolithography prcoess and lift-off techniques. The Ti/Au metal forms a good ohmic contact with β-Ga_2O_3 film. The dark current and photocurrent are linearly related to bias voltage in a linear coordinate system. Figure 5 describes the *I*–*V* characteristics in dark and under UV (254 nm) illumination for different thicknesses with the voltages sweeping from 0 V to 10 V in steps of 100 mV. The dark current changes little for the three samples, while the photocurrent increases exponentially with the increase of number of growth cycles. The ultra-low dark currents of these samples (134 fA, 363 fA, and 234 fA) at a bias voltage of 10 V indicate that the low oxygen vacancy concentration exists in the β-Ga_2O_3 film grown by ALD using ozone as an oxygen source.[20] The photocurrent I_{photo} is 5.27×10^{-10} A of sample 1, 2.99×10^{-8} A of sample 2, and 2.11×10^{-6} A of sample 3 at bias of 10 V, separately. As the thickness of the film increases, the light absorption layer thickens. Thus the number of photon-generated carriers increases greatly. It is worth noting that when the thickness increases linearly in a range of 18 nm–58 nm, the photocurrent I_{photo} shows an almost exponential increase.

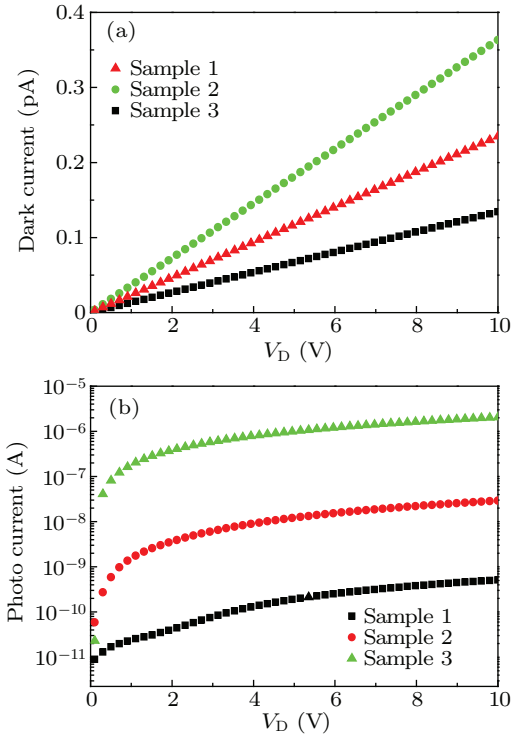


Fig. 5. The *I*–*V* characteristic curves of β-Ga_2O_3 MSM PD for samples 1, 2, and 3: (a) dark currents in linear coordinate and (b) the photocurrents under 254-nm UV light illumination in exponential coordinate.

In order to further explore the photoelectric response performance, we also calculate the photo-to-dark current ratio ($I_{\text{photo}}/I_{\text{dark}}$, PDCR), light responsivity (R), external quantum efficiency (EQE), and detectivity (D^*) to compare the performance parameters of these devices. The responsivity (R) is related to the irradiation intensity (P) and effective radiation area (S), and given by[21]

$$R = \frac{(I_{\text{photo}} - I_{\text{dark}})}{(P \cdot S)}. \tag{2}$$

The external quantum efficiency (EQE) is defined as the ratio of the number of electrons collected by the detector's electrodes to the number of photons received, and can be expressed as

$$\text{EQE} = \frac{h\nu R}{q}, \tag{3}$$

where $h\nu$ represents the photo's energy[22] and q is the electron charge of 1.6×10^{-19} C. The specific detectivity (D^*) refers the detection rate of the device per unit device area and 1-Hz measuring band width. The higher the D^*, the stronger the ability to detect the weak signals for photodetectors. The specific detectivity (D^*) can be obtained from the following equation:

$$D^* = \frac{R}{\sqrt{2qI_{\text{dark}}/S}}. \tag{4}$$

Figure 6 shows the key parameters of the three samples at room temperature extracted from the *I*–*V* characteristics. For sample 3, the photo-to-dark current ratio (PDCR) at 10 V reaches 1.57×10^7, while only 2.25×10^3 for sample 1. The high light–dark current ratio indicates that the device has high sensitivity and great application potentials in photoelectric detectors. In addition, with the number of growth cycles increasing, the responsivity increases from 3.90×10^{-4} A/W for sample 1, to 1.56 A/W for sample 3. The EQE increases from 0.19% to 764.49%. Meanwhile, the detectivity (D^*) increases from 5.24×10^{10} Jones to 2.44×10^{14} Jones. As the thickness of the film increases, the light absorption capacity of the film gradually increases. So the parameters relating to photocurrent increase significantly with film thickness as shown in Fig. 6.

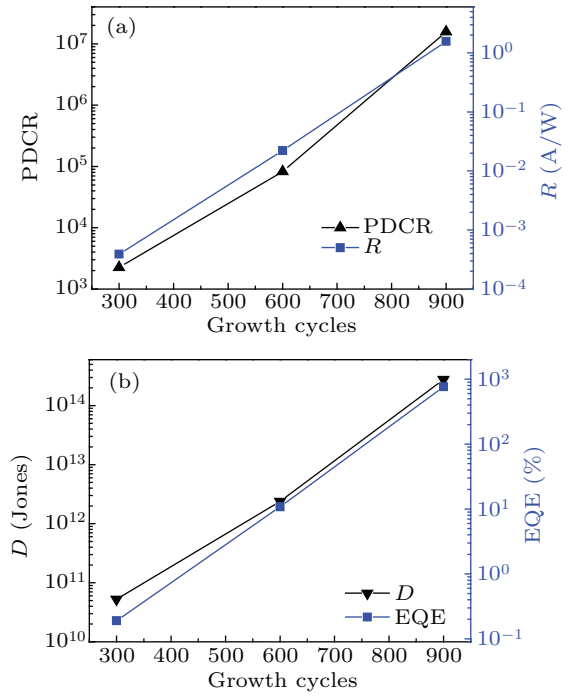


Fig. 6. Dependence of (a) PDCR and responsivity (b) detctivity and external quantum efficiency on the number of grown cycles, with *y*-coordinate being exponential.

In addition, the time-dependent light response characteristics under 254-nm DUV illumination are studied by switching the UV light source. After several photo switch cycles, the MSM PD still exhibits almost the same photocurrent as shown in Figs. 7(a)–7(c). The time–response curves of single on/off cycle for three samples are shown in Figs. 7(d)–7(f). The rising section and falling section of a single cycle response curve can be fitted by double exponential equation and described as follows:

$$I = I_0 + A\,\mathrm{e}^{-t/\tau_1} + B\,\mathrm{e}^{-t/\tau_2}, \tag{5}$$

where I is stable state photocurrent, A and B are the fitting constants, and τ_1 and τ_2 represent two time constants (fast response time and slow response time).[16] The fast response times are related to the direct band-to-band transition, while the slow response times may be related to the carrier trapping/de-trapping mechanism. The τ_r and τ_f are the rising

and decay edges of the time constants, respectively. Time relaxation constants under 254-nm exposure are 0.40 s (τ_{r1}) and 1.94 s (τ_{r2}) for sample 1, 0.48 s (τ_{r1}) and 2.43 s (τ_{r2}) for sample 2, while the same values of τ_{r1} and τ_{r2} ($\tau_{r1} = \tau_{r2} = 0.25$ s) are obtained for sample 3 by fitting the experimental data using Eq. (5). So only the fast response component exists when the 254-nm UV light is switched on, which indicates a low trap density for sample 3. When the UV light is switched off, the current falls very rapidly. The two components (τ_{d1} and τ_{d2}) have the same value τ_d obtained by fitting the experiment data by Eq. (5). The decay time constant τ_d is 0.08 s for sample 1, 0.069 s for sample 2, and 0.045 s for sample 3.

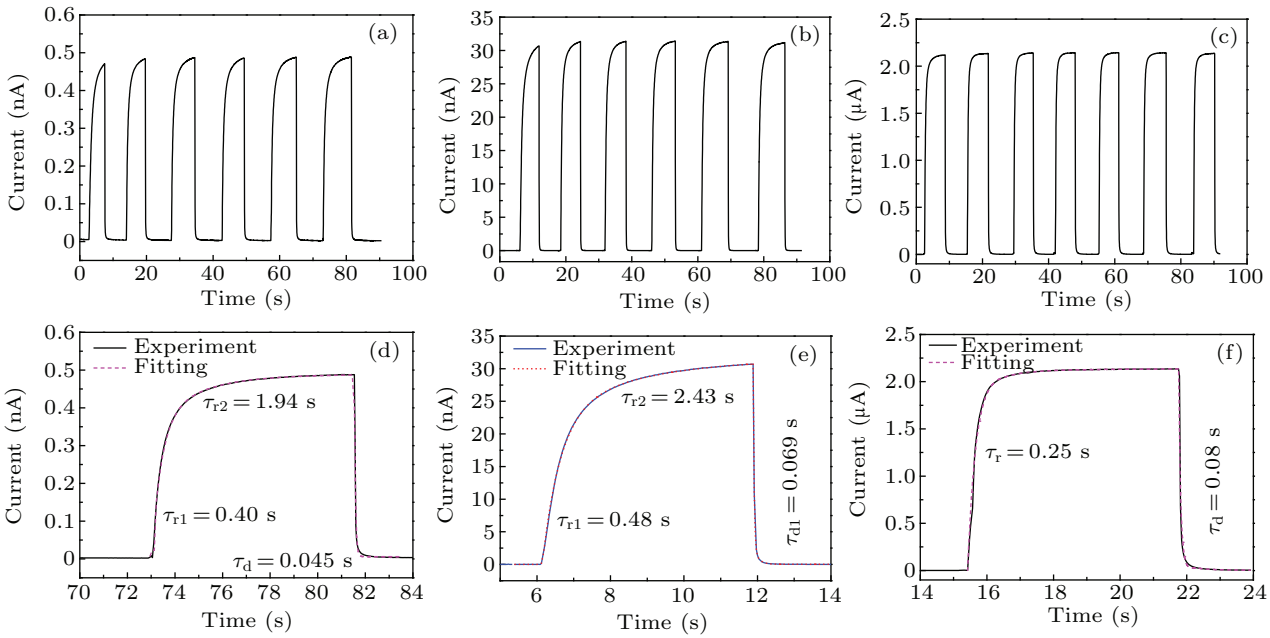


Fig. 7. Photoresponse of MSM PDs of (a) sample 1, (b) sample 2, and (c) sample 3. Partial enlargement of the transient response curves under 254-nm light and the fitting curve of the double exponential relaxation equation of (d) sample 1, (e) sample 2, and (f) sample 3.

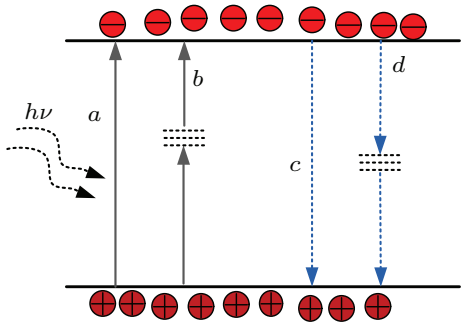


Fig. 8. Schematic illustration of energy band relating to carrier generation mechanism and recombination mechanism for β-Ga_2O_3 photodetectors.[25]

In order to fully understand the mechanism of the rise and decay process, it can be explained in terms of the mechanism of carrier generation and recombination,[23–25] as shown in Fig. 8. Generally, because the photon energy of 254-nm UV light is 4.88 eV, which is nearly equal to the band gap of β-Ga_2O_3. The electrons in the valence band will be excited by the photon, transforming into photocarriers as shown in process *a* of Fig. 8. But some of these excited electrons may be captured by traps, and then the electron–hole pair will be generated by the transition from the trap level to the conduction band again as shown in process *b*. Thus, the trapping process caused will lead to an increase of the rise time of Ga_2O_3 photoelectric detector. In our work, the polycrystalline β-Ga_2O_3 films for the three samples exhibit more grain boundaries, which leads to an increased probability of carrier being captured by the trap levels.[26] With the decrease of gallium oxide thickness, the density of trap centers caused by grain boundary becomes more obvious, which can be inferred from SEM images. As a result, the rise time for the sample 1 and sample 2 are both more longer than that of sample 3.

When the UV light is turned off, the non-equilibrium carriers recombine with the holes in the valence band to complete the inter-band annihilation process as shown in process *c*. Also, the some of these non-equilibrium electrons will recombine with the holes through the bulk or surface recombination centers, as shown in process *d*. From Fig. 7, we can find that the thinner the Ga_2O_3 film, the shorter the decay time is. We can attribute the decrease of decay time to strong surface recombination effect when the thickness of thin film decreases.[27–29] At the surface of semiconductor materials, there is also composite mechanism that reduces the lifetime of photogenerated carrier. The surface states are located in the band gap and usually act as a recombination center. Owing to the surface-to-volume ratio increasing with the thickness of film decreasing, surface recombination effect turns stronger. Therefore, as the film thickness decreases, the decay time de-

creases.

For contrast, the photoresponse of MSM PDs with a 58-nm-thick β-Ga_2O_3 film is measured under 365-nm UV illumination, and the results are shown in Fig. 9. The photocurrent is 2.28×10^{-12} A at 10 V. The I_{photo}/I_{dark} is about 17.9 under 365-nm UV light illumination with an intensity of 1120 μW/cm^2, corresponding to 8.3×10^{-6} A/W of photo responsivity. According to the responsivity of 254 nm/365 nm, the photoresponse rejection ratio (R_{254}/R_{365}) reaches up to 1.86×10^5.

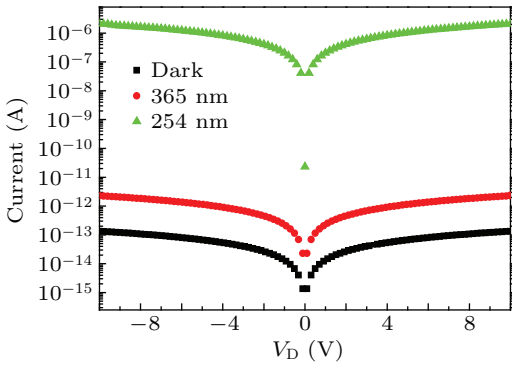


Fig. 9. Three *I*–*V* curves of β-Ga_2O_3 MSM PD with 58-nm-thick Ga_2O_3 film in the dark, under 365-nm and 254-nm UV light illuminations, respectively.

3.3. Dependence of innerfinger spacing on photoelectric performance

In order to study the influence of size on the performance of photodetector, we fabricate MSM photodetectors with different interfinger spacings (50 μm, 40 μm, 30 μm, 20 μm, and 10 μm) in sample 3 (corresponding to a β-Ga_2O_3 film thickness of 58 nm). The number of fingers and the finger widths are fixed at 5 μm and 300 μm, respectively. The *I*–*V* characteristics of Ga_2O_3 MSM PD in the dark and 254-nm illumination are shown in Figs. 10(a) and 10(b).

As shown in Fig. 10 and Table 1, both the photo current and dark current increase gradually with the decrease of the interfinger spacing, which can be attributed to the reduction of carrier transport time from source electrode to drain electrode. All the parameters (photoresponsivity, detectivity, and external quantum efficiency) increase with the decrease of interfinger spacing, while there is no regular change for the PDCR. The photocurrent of 5.4 μA, photo-to-dark current ratio of 4.90×10^6, photoresponsivity of 20 A/W, specific detectivity of 5.54×10^{14} Jones, and external quantum efficiency of 9780% are all obtained for the MSM PD with 10-μm spacing under 254-nm UV light illumination.

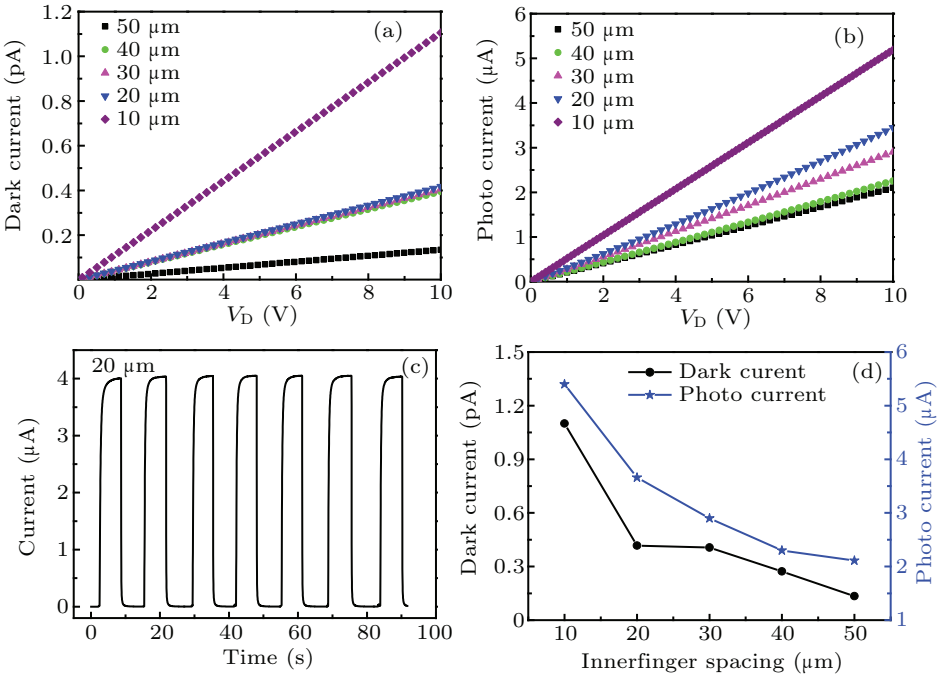


Fig. 10. Current–voltage (*I*–*V*) characteristics curves of Ga_2O_3 MSM PD (a) in dark and (b) under 254-nm illumination; (c) time-dependent photoresponse of MSM PD with 20-μm-innerfinger spacing under 254-nm illumination, and (d) dependence of photo current and dark current on interfinger spacing at bias voltage of 10 V.

Table 1. Key parameters extracted from *I*–*V* characteristics for five devices.

Finger spacing	50 μm	40 μm	30 μm	20 μm	10 μm
I_{dark} (A)	1.34×10^{-13}	2.72×10^{-13}	4.06×10^{-13}	4.17×10^{-13}	1.10×10^{-12}
I_{light} (A)	2.11×10^{-6}	2.30×10^{-6}	2.90×10^{-6}	3.94×10^{-6}	5.40×10^{-6}
PDCR	1.57×10^7	7.50×10^6	7.10×10^6	9.4×10^6	4.90×10^6
R (A/W)	1.56	2.13	3.58	7.29	20.00
D^* (Jones)	2.77×10^{14}	2.37×10^{14}	2.83×10^{14}	4.64×10^{14}	5.54×10^{14}
EQE (%)	7.64×10^2	1.04×10^3	1.75×10^3	3.57×10^3	9.78×10^3

4. Conclusions

In this work, the solar-blind UV photodetectors with high PDCR and ultra-low dark current are fabricated on β-Ga_2O_3 films by ozone-based ALD process. The effects of thin film thickness on the performances of β-Ga_2O_3 photodetectors are investigated. Except for the dark current, the detection performances (light–dark current ratio, responsivity, specific detectivity, external quantum efficiency) of the solar blind photodetector almost increase exponentially with the increase of the film thickness. The β-Ga_2O_3 UV photodetector with a thickness of 58-nm exhibits a very low dark current of 134 fA and a high light–dark current ratio of 1.57×10^7 at a 10-V bias voltage. The photoresponse rejection ratio (R_{254}/R_{365}) is up to 1.86×10^5 for the photodetectors with a finger spacing of 50 μm. The relationship between finger spacing and photoelectric parameters is also studied. All of the photoelectrical parameters but for PDCR increase with the decrease of interfinger spacing. The responsivity uner 254-nm light illumination is 20 A/W for the MSM device with 10-μm finger spacing. Therefore, both the film thickness and innerfinger spacing are sensitive parameters affecting the performance of solar blind photoelectric detector. This study provides an effective and simple method for improving photoelectric performance of Ga_2O_3-based MSM PDs.

Acknowledgements

Project supported by the Natural Science Basic Research Program of Shaanxi Province, China (Grant No. 2022JQ-701) and the Scientific Research Program Funded by Shaanxi Provincial Education Department, China (Grant No. 21JK0919).

References

[1] Pearton S J, Yang J C, Cary IV P H, Ren F, Kim J, Tadjer M J and Mastro M A 2018 *Appl. Phys. Rev.* **5** 011301
[2] Baldini M, Galazka Z and Wagner G 2018 *Mater. Sci. Semicond. Proc.* **78** 132
[3] Hao W B, He Q M, Zhou K, Xu G W, Xiong W H, Zhou X Z, Jian G Z, Chen C, Zhao X L and Long S B 2021 *Appl. Phys. Lett.* **118** 043501
[4] Zhong M Z, Wei Z M, Meng X Q, Wu F M and Li J B 2015 *J. Alloys Compd.* **619** 572
[5] Ogita M, Higo K, Nakanishi Y and Hatanaka Y 2001 *Appl. Surf. Sci.* **175** 721
[6] Yoshioka S, Hayashi H, Kuwabara A, Oba F, Matsunaga K and Tanaka I 2007 *J. Phys.: Condens. Matter* **19** 346211
[7] Xie C, Lu X T, Tong X W, Zhang Z X, Liang F X, Liang L and Luo L B 2019 *Adv. Fuct. Mater.* **29** 1806006
[8] Lee S H, Kim S B, Moon Y J, Kim S M, Jung H J, Seo M S, Lee K M, Kim S K and Lee S W 2017 *ACS Photon.* **4** 2937
[9] Feng Z X, Anhar Uddin Bhuiyan A F M, Karim M R and Zhao H P 2019 *Appl. Phys. Lett.* **114** 250601
[10] Yu F P, Ou S L and Wu D S 2015 *Opt. Mater. Express* **5** 1240
[11] Sasaki K, Kuramata A, Masui T, Villora E G, Shimamura K and Yamakoshi S 2012 *Appl. Phys. Express* **5** 035502
[12] Cheng Y L, Xu Y, Li Z, Zhang J Q, Chen D Z, Feng Q, Xu S R, Zhou H, Zhang J C, Hao Y and Zhang C F 2022 *J. Alloys Compd.* **831** 154776
[13] Saikumar A K, Nehate S D and Sundaram K B 2019 *ECS J. Solid Sci. Technol.* **8** Q3064
[14] Shen H, Baskaran K, Yin Y, Tian K, Duan L B, Zhao X R and Tiwari A 2020 *J. Alloys Compd.* **822** 153419
[15] Zhang X Y, Wang L, Wang X D, Chen Y, Shao Q Q, Wu G J, Wang X Y, Lin T, Shen H, Wang J L, Meng X J and Chu J H 2020 *Opt. Express* **28** 4169
[16] An Y H, Zhi Y S, Cui W, Zhao X L, Wu Z P, Guo D Y, Li P G and Tang W H 2017 *J. Nanosci. Nanotechnol.* **17** 9091
[17] Li X H, Zhang M, Yang J, Xin S, Gao Y, Li Y Z, Li S Y and Wang C J 2022 *Acta Phys. Sin.* **71** 048501 (in Chinese)
[18] Sun R, Zhang H Y, Wang G G, Han J C, Wang X Z, Cui L, Kuang X P, Zhu C and Jin L 2014 *Superlattices Microst.* **65** 146
[19] Jubu P R, Yam F K, Igba V M and Beh K P 2020 *J. Solid State Chem.* **290** 121576
[20] An Y H, Guo D Y, Li S Y, Wu Z P, Huang Y Q, Li P G, Li L H and Tang W H 2016 *J. Phys. D: Appl. Phys.* **49** 285111
[21] Liu Z, Zhi Y S, Li S, Liu Y Y, Tang X, Yan Z Y, Li P G, Li X H, Guo D Y, Wu Z P and Tang W H 2019 *J. Phys. D: Appl. Phys.* **53** 085105
[22] Wang J, Xiong Y Q, Ye L J, Li W J, Qin G P, Ruan H B, Zhang H, Fang L, Kong C Y and Li H L 2021 *Opt. Mater.* **112** 110808
[23] Li L, Auer E, Liao M Y, Fang X S, Zhai T Y, Gautam U K, Lugstein A, Koide Y, Bando Y and Golberg D 2011 *Nanoscale* **3** 1120
[24] Guo D Y, Wu Z P, An Y H, Guo X C, Chu X L, Sun C L and Li L H 2014 *Appl. Phys. Lett.* **105** 023507
[25] Liu X Z, Liu Q, Zhao B W, Ren Y X, Tao B W and Zhang W L 2020 *Vaccum* **178** 109435
[26] Ma M H, Zhang D, Li Y Q, Lin R C, Zheng W and Huang F 2019 *ACS Appl. Electron. Mater.* **1** 1653
[27] Guo X C, Hao N H, Guo D Y, Wu Z P, An Y H, Chu X L, Li L H, Li P G, Lei M and Tang W H 2016 *J. Alloys Compd.* **660** 136
[28] Dan Y P, Seo K, Takei K, Meza J H, Javey A and Crozier K B 2011 *Nano Lett.* **11** 2527
[29] Liang Z M, Zeng P Y, Liu P Y, Zhao C X, Xie W G and Mai W J 2016 *ACS Appl. Mater. Inter.* **8** 19158